Computational imaging of aortic vasa vasorum and neovascularization in rabbits using contrast-enhanced intravascular ultrasound: Association with histological analysis

Manolis Vavuranakis[#], Theodore G. Papaioannou[#], Dimitrios Vrachatis,
Michael Katsimboulas[1], Elias A. Sanidas[2], Sophia Vaina, George Agrogiannis[3],
Efstratios Patsouris[3], Ioannis Kakadiaris[4], Christodoulos Stefanadis, Dimitrios Tousoulis

First Department of Cardiology, Hippokration Hospital, Biomedical Engineering Unit, Medical School,
National and Kapodistrian University; Athens-*Greece*
[1]Centre of Clinical, Experimental Surgery and Translational Research, Experimental Surgery Unit,
Biomedical Research Foundation of the Academy of Athens; Athens-*Greece*
[2]Department of Cardiology, "Laiko" General Hospital; Athens-*Greece*
[3]Department of Pathology, Medical School, National and Kapodistrian University; Athens-*Greece*
[4]Computational Biomedicine Lab, Department of Computer Science, University of Houston; TX-*USA*

ABSTRACT

Objective: Neoangiogenesis is pathophysiologically related to atherosclerotic plaque growth and vulnerability. We examined the *in vivo* performance of a computational method using contrast-enhanced intravascular ultrasound (CE-IVUS) to detect and quantify aortic wall neovascularization in rabbits. We also compared these findings with histological data.

Methods: Nine rabbits were fed with a hyperlipidemic diet. IVUS image sequences were continuously recorded before and after the injection of a contrast agent. Mean enhancement of intensity of a region of interest (MEIR) was calculated using differential imaging algorithm. The percent difference of MEIR before and after the injection of microbubbles (d_MEIR) was used as an index of the density of plaque or/and adventitial neovascularization. Aortic segments were excised for histological analysis.

Results: CE-IVUS and histological analysis were performed in 11 arterial segments. MEIR was significantly increased (~20%) after microbubble injection (from 8.1±0.9 to 9.7±1.8, p=0.016). Segments with increased VV/neovessels in the tunica adventitia (histological scores 2 and 3) had significantly higher d_MEIR compared with segments with low presence of VV/neovessels (score 1); 40.5±22.9 vs. 8±14.6, p=0.024, respectively.

Conclusion: It is possible to detect VV or neovessels *in vivo* using computational analysis of CE-IVUS images, which is in agreement with histological data. These findings may have critical implications on vulnerable plaque assessment and risk stratification. *(Anatol J Cardiol 2018; 20: 117-24)*

Keywords: neoangiogenesis, microbubbles, vulnerable plaque, aorta, atherosclerosis

Introduction

Although the most widely accepted parameter characterizing atherosclerotic plaque severity is stenosis degree, other additional features assessing plaque morphology, functionality, and composition have been recognized as significant factors (1-3). In particular, the proliferation of vasa vasorum and neoangiogenesis (or neovascularization) within the plaque area have been linked to atherosclerotic plaque growth and instability (4, 5). The presence and the extent of plaque neovascularization have been associated with clinical symptoms (6, 7) as well as with cardiovascular risk (8); therefore, they represent clinically relevant biomarkers.

Several recent methods and techniques are now available for the *in vivo* imaging and assessment of the extent of vasa vasorum and plaque neovascularization; some of them are based on magnetic resonance imaging, computed tomography,

118 Vavuranakis et al.
Vasa vasorum imaging by contrast enhanced IVUS

Anatol J Cardiol 2018; 20: 117-24
DOI:10.14744/AnatolJCardiol.2018.35761

positron emission tomography (9-11), but contrast-enhanced ultrasound (CEUS) imaging is undoubtedly the most widely used technique (12, 13) apart from intravascular ultrasound (14-16). Methods using CEUS are based on the use of contrast medium (microbubbles) that can cause changes in the echolucency and echogenicity of arterial wall and plaque regions of interest (ROI) yielding qualitative, semiquantitative, and quantitative information regarding the presence and the extent of vasa vasorum and neovascularization. Nevertheless, there are very limited data from validation studies examining the accuracy of these CEUS imaging methods in comparison to histological data (12).

A new method has been previously described for the qualitative and quantitative assessment of vasa vasorum and plaque neovascularization *in vivo*. This method uses a differential computational analysis (17, 18) of contrast-enhanced intravascular ultrasound (CE-IVUS) image sequences, before and after the injection of microbubbles (17, 19). The aim of the present study was to evaluate *in vivo* the performance of this computational technique using CE-IVUS to detect and quantify aortic wall neovascularization in rabbits and also to explore any possible association between imaging markers of neovascularization with histological data.

Methods

Study protocol

The study used an animal model of atherosclerosis mainly based on a 3-month high cholesterol diet. Thus, following an acclimatization period of 1 week of being housed under standard laboratory conditions, 10 male White New Zealand rabbits (Rbs; Trompetas Breeding Laboratories; Attiki, Greece), with an average body weight (BW) of 2.8±0.15 kg, received an atherogenic diet containing 1% cholesterol (Mucedola, Italy). Food consumption was recorded daily (250±50 g chow/day/animal), and BW was measured monthly. In four animals, to accelerate processes of atheromatosis, a balloon-induced injury of the aortic endothelium was induced by a 4 F Fogarty catheter 1 week after the initiation of diet. The balloon of the Fogarty catheter was inflated under fluoroscopy. When aortic wall stretching was visible, then the catheter was pulled along the aorta while still inflated. The rest six animals were only fed with the atherogenic diet. At the end of the experimental period, all animals were euthanized with an intravenous overdose of sodium pentobarbital (120 mg/kg).

Starting 12 h before surgery, all animals were maintained on a water-only diet. All animals received antibiotic prophylaxis with a single dose of cefuroxime sodium (25 mg/kg, Zinacef; GlaxoSmithKline, Brentford, UK) intravenously administered 30 min before surgery, and Lactated Ringer's solution was administered intravenously at a rate of 10 ml/kg/h. All surgical procedures were performed by the same surgeon (MK). Animals

were preanesthetized with ketamine (35 mg/kg, Imalgene 1000; Merial, Lyon, France) and xylazine (5 mg/kg, Rompun; Bayer Animal Health, Leverkusen, Germany) via intramuscular administration. After tracheal intubation, they were connected to a veterinary ventilator (MDS Matrix Model 2000; Hallowell EMC, Pittsfield, MA) and general anesthesia was maintained by sevoflurane (3% Sevorane; Abbott, UK). Following anesthesia, each animal was placed in a dorsal recumbent position. A surgical scrub of the proposed surgical site was performed using povidone iodine scrub and alcohol. A 2-cm vertical midline incision of the right ventral femoral area was performed after injection of 2-3 ml of 2% lidocaine (Xylocaine, Astra Zeneca). The right femoral artery was identified, dissected, and temporarily legated at its distal end. A cutdown was performed to place a 5-Fr introducer sheath (Avanti+, Cordis Europa, NL) proximally under radiological control (C arm, BV Libra, Philips Medical Systems, Da Best, The Netherlands). A diagnostic angiogram of the abdominal aorta was performed through the sheath.

CE-IVUS was performed for every plaque that we identified. Plaques under evaluation were marked by clips inserted externally by the surgeon on the aortic wall under fluoroscopic and IVUS guidance. Finally the aortic trunk containing all studied plaques was completely excised. Overall, 11 aortic segments were obtained. Paraffin wax (impregnation) and histological assessment was performed.

Contrast-enhanced intravascular ultrasound

Instrumentation for intravascular imaging instrumentation was performed in deep protocol anesthesia. For each animal, IVUS imaging was performed (Invision; Volcano Therapeutics, Rancho Cordova, CA) by an intracoronary phased array catheter (Avanar®, F/X) for detecting atherosclerotic aortic lesions. The acoustic output parameters of this catheter were the following: central frequency (f)=20 MHz, derated peak negative pressure (DPNP) at a location of the maximum derated pulse intensity integral=0.07 MPa and mechanical index=0.035. Mechanical index was defined as $MI=DPNP/(f^{1/2})$ (20). CE-IVUS was performed in three phases for each animal: (i) typical grayscale IVUS imaging along the aorta was performed by manual pullback of the IVUS catheter for detecting the atherosclerotic lesions before they were excised for histological analysis. (ii) After the localization of the target aortic segment, the IVUS catheter was stabilized and a first baseline IVUS loop was continuously recorded for 15–20 s (before the injection of contrast media). (iii) After the baseline recording, a solution of microbubbles was injected through the guiding catheter and CE-IVUS imaging at the same location was continued for at least 60 s. The Sonovue® solution (Bracco Altana Pharma, Germany) was used (0.06 ml/kg) for contrast enhancement. Sonovue® is a contrast agent for ultrasonography, which is an aqueous suspension of stabilized SF6 microbubbles (phospholipid-stabilized microbubbles of sulfur hexafluoride). The size of these microbubbles was 1-10 μm and their number is approximately $2-5\times10^8$ per ml.

Anatol J Cardiol 2018; 20: 117-24
DOI:10.14744/AnatolJCardiol.2018.35761

Vavuranakis et al.
Vasa vasorum imaging by contrast enhanced IVUS   *119*

Imaging of vasa vasorum and neoangiogenesis

IVUS image sequences were continuously recorded before and after the injection of microbubbles. The recorded IVUS loops were transferred in DICOM format to a PC for further processing. Each loop was analyzed using an automated algorithm, which has been previously described and proposed for quantification and visualization of vasa vasorum and plaque neovascularization (14, 17). The method is based on the detection of the enhancement in the intensity of specific ROI determined by the user (ACES™ software-Analysis of Contrast-Enhanced Sequences, Computational Biomedicine Lab, Dept. of Computer Science, Houston University, TX, USA) as previously described in detail (18, 21). A baseline (precontrast) image is derived by averaging the preinjection "stabilized" image sequence, which was derived after appropriate processing for the elimination of aortic wall movement. Then, this average image is subtracted from all frames in the sequence, producing a sequence of difference images. When changes occur because of contrast enhancement (i.e., where microbubbles are visible), a positive difference can be subsequently quantified and visualized. To quantify enhancement in a particular frame, we averaged the gray levels of the difference image over the ROI producing the MEIR statistic (mean enhancement of intensity in ROI) (14, 17, 18). This procedure was repeated for all frames. The percent difference of MEIR before and after the injection of microbubbles (d_MEIR) was used as an index of the density of plaque or/and adventitial neovascularization.

Differential computational imaging algorithm

An automatic algorithm (ACES: Analysis of Contrast-Enhanced Sequences, Computational Biomedicine Lab, Dept. of Computer Science, Houston University, TX, USA) has been previously developed and described in detail for the quantification and visualization of VV in CE-IVUS image sequences (21, 18). This technique is based on the detection of local echogenicity changes (because of the perfusion of microbubbles into the aortic wall) in stationary IVUS sequences. The detection of intensity enhancement of the selected ROI is performed offline and consists of the following steps:

(a) At first, any motion artifacts caused by cardiac contractions are eliminated from the IVUS sequence using a sequence-gating algorithm, which is automatically driven by the imaging data; it is based on the analysis of the interframe correlations with a standard registration metric (18, 22). This task is accomplished by transforming the image sequence to a Euclidean multidimensional similarity space in which each frame is represented by a particular, although not necessarily unique, point; this space is clustered using k-means (with multiple runs to achieve the lowest error) to provide an ensemble of stabilized frames (18). Typically, the operator selects the number of clusters to use from a visualization of the clusters associated with several k as there is a tradeoff between a high value, which imposes greater restrictions on which frames are

considered to be similar, and a low value, which forces some events which could be considered distinct to coalesce (18). The frames of the selected cluster are then used to build a new sequence for which it is assumed that the axial catheter motion has essentially been eliminated (18).

(b) After that, the area of interest is manually defined by the operator by tracing the luminal and media/adventitia contours in the first frame of the gated image sequence. The ROI corresponding to each frame in the gated sequence is located and "unwrapped" into a rectangular domain (18). To eliminate any remaining motion artifacts, the images are aligned and superimposed to obtain a pixelwise correspondence using a two-step approach that consists of a rough, rigid alignment step followed by an elastic refinement step (18). A precontrast baseline image is computed by averaging the subset of gated frames corresponding to the period before the injection of microbubbles (18). The precontrast baseline image is subtracted from all frames in the gated sequence to form the differential images where spots of enhancement are visualized by different colors using a color scale from blue (no difference) to red (highest difference). As a result, any change that occurs because of contrast enhancement will be reflected as a positive difference in the intensities in the corresponding regions of the differential images (18). As mentioned earlier, the enhancement in a particular frame is computed by averaging the gray levels of the difference image over the ROI, which provides the Mean Enhancement of Intensity of the Region of Interest (MEIR). The difference of the MEIR of baseline images from the MEIR of postinjection (microbubbles) images expressed as a percentage (d_MEIR) was finally used as an index of the VV or neovascularization density at the region of interest.

Surgical exertion and histological analysis of aortic segments

Aortic segments were excised for histological analysis primarily aiming to detect neovessels developed at the plaque or adventitial regions. Previous IVUS and OCT *in vivo* studies in which interventional techniques (including pathological examination of the specimens) were used or *in vivo* follow-up studies in humans have addressed that there is a great uncertainty whether the IVUS or OCT imaging plane is exactly the same with the tissue plane that is examined histologically or at follow-up (23, 24). To overcome this limitation, we used surgical clips that were inserted at the aortic wall under simultaneous IVUS imaging guidance, to match the imaged plaque or aortic segment with the one examined histologically. Then, the following stainings were performed: CD34 for endothelial cells, CD68 for macrophage, CD3 for lymphocytes and staining with antibody against von Willebrand factor (25-27). Routine staining was also performed by hematoxylin and eosin (H&E) (28).

Statistical analysis

The continuous variables of the study were presented as mean, median, standard deviation, and interquartile range val-

120 Vavuranakis et al.
Vasa vasorum imaging by contrast enhanced IVUS

Anatol J Cardiol 2018; 20: 117-24
DOI:10.14744/AnatolJCardiol.2018.35761

ues. Semiquantitative and qualitative categorical variables were presented as absolute frequencies and percentages. The difference in MEIR before and after the injection of microbubbles was evaluated by the nonparametric Wilcoxon test. The d_MEIR index of segments with low-grade neovascularization as determined by histological evaluation was compared with d_MEIR of the respective segments with high-grade neovascularization by using the nonparametric Mann–Whitney U test. The association between d_MEIR and the histological evidence of the extent of VV/neovascularization at the areas of interest in the media and adventitia was assessed using the nonparametric Spearman correlation coefficient. Statistical significance was accepted for a p value of <0.05. The statistical analysis was performed using the IBM SPSS Statistics for Windows software (vs. 21, IBM Corp., Armonk, NY: USA).

Results

In each animal, at least one atherosclerotic plaque was examined after it was identified by IVUS. Out of the 10 animals that were initially included in the study, three were excluded: one animal died before the follow-up examination and another did not develop any atherosclerotic lesion; the IVUS apparatus malfunctioned during the follow-up examination in the third animal. Therefore, we finally investigated 11 different atherosclerotic aortic lesions from seven animals. Focal disease was detected in all animals mostly in the lower thoracic and upper abdominal aorta, but most of the plaques were not impressive, except in two cases.

CE-IVUS and histological analysis was eventually performed in 11 arterial segments (1 with foam cells, nine with pathological intimal thickening, and one with fibroatheroma). The presence and density of VV or/and neovessels was assessed using a semiquantitative scoring system (0–3) as described previously (29). Separate analysis was performed for VV/neovessels presence at (i) the media, (ii) the adventitia, and (iii) the plaque area. Seven adventitial segments had score of 1, one had score of 2, and three had a score of 3. Six segments had no presence of VV at the arterial wall media, three segments had a score of 1, and two segments had a score of 2. Finally, only one segment had small number of neovessels developed within the plaque area (score 1). Histological findings and observations are presented in Table 1, and two representative cases of vasa vasorum imaging are illustrated at Figure 1. In particular, the detected VV or neovessels by histological analysis and by computational image analysis of CE-IVUS images are shown by red spots in two cases: one with extended neovascularization (Case 1) and one with moderate extent of neovascularization (Case 2).

MEIR was computed for a region of interest that included plaque (if existed) in the media and adventitia. MEIR was significantly increased (by approximately 20%) after microbubble
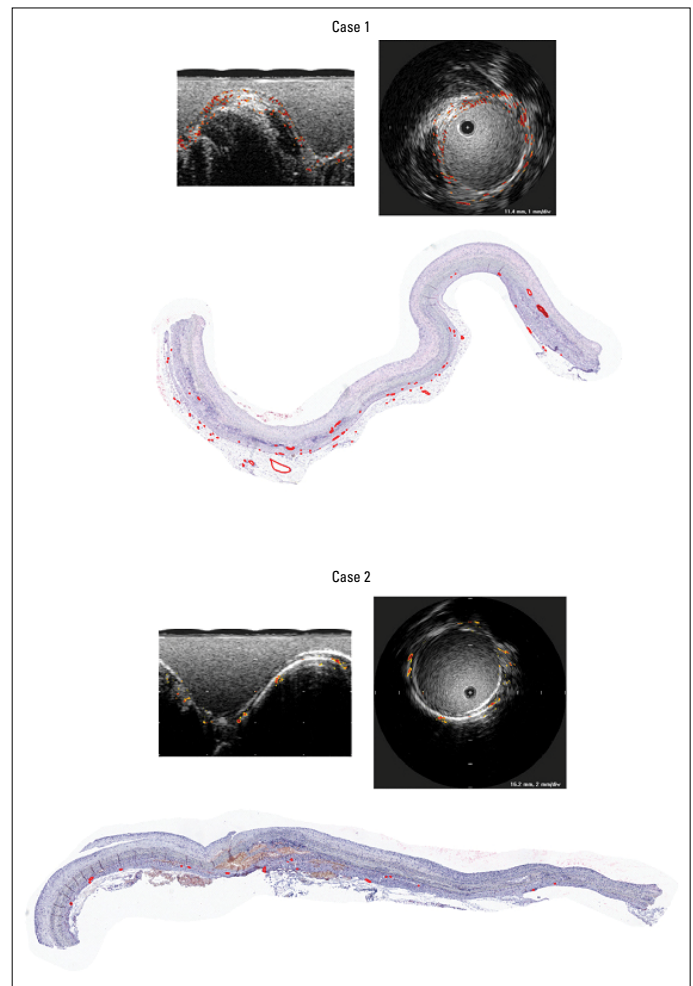

Figure 1. Computational imaging by CEUS and histological evidence of vasa vasorum and neovascularization are shown for two cases with high (Case 1) and low (Case 2) degree of neovascularization. The upper two images for each case correspond to different views of the processed CE-IVUS images and the image below depicts the histological evidence of VV/neovessels after the proper staining

injection (from 8.1±0.9 to 9.7±1.8, p=0.016). In general, the extent of VV/neovascularization from the d_MEIR was significantly correlated with the histological evidence score (r=0.768, p=0.006) for the ROIs corresponding to the adventitia of the examined aortic segments; however, no significant correlation was observed for the media area (r=0.367, p=0.267). Segments with increased VV/neovessels at the adventitia (histological scores 2 and 3) had significantly higher d_MEIR than segments with low presence of VV/neovessels (score 1); 40.5±22.9 vs. 8±14.6, p=0.024, respectively.

Discussion

The primary finding of the present study is that "visualization" and quantification of VV and/or neovessels of atherosclerotic plaques are feasible with the utilization of an automated

Anatol J Cardiol 2018; 20: 117-24
DOI:10.14744/AnatolJCardiol.2018.35761

Vavuranakis et al.
Vasa vasorum imaging by contrast enhanced IVUS   *121*

Table 1. Histological data and macroscopic features for each examined atherosclerotic aortic lesion

Animal#/Lesion#	Plq/Med ratio*	Plaque type	Calcium	Chol crystals	Microvessels in plaque	Microvessels in media	Microvessels in adventitia	Comments
Animal-1 Lesion-1	0.5/1	FC	0	0	0	0	(+)	Probably normal vasa vasorum in adventitia
Animal-2 Lesion-1	1/1	PIT	0	0	0	0	+	Mostly foam cells
Animal-2 Lesion-2	2.5/1	PIT	0	0	0	0	++ focally	Microvessels focally in adventitia beneath thickest part of plaque
Animal-3 Lesion-1	4/1	FA	+++ media	++	+	++	+++	Thick cap of SMC (balloon injury?)
Animal-4 Lesion-1	1.5/1	PIT	++ intima	+	0	+	+++	Normal, very thick media The many adventitial microvessels might be normal
Animal-4 Lesion-2	2/1	PIT	+++ media	+	0	++	+	Severe medial damage with dense calcification and foam cells
Animal-4 Lesion-3	1.5/1	PIT	+++ media	0	0	+	+++	
Animal-4 Lesion-4	1/1	PIT	+++ media	0	0	+	+	Dense medial calcification
Animal-5 Lesion-1	<1/1	PIT	0	0	0	0	+	
Animal-6 Lesion-1	<1/1	PIT	0	0	0	0	++ focally	(Surface endothelium is missing)
Animal-7 Lesion-1	<0.5/1	PIT	0	0	0	0	+++ focally	Very small intimal lesions

#stands for id
(code number for each animal and each lesion)
*Plaque/media thickness ratio estimated visually where intima is thickest
FC=foam cell lesion (few smooth muscle cells (SMC) and sparse extracellular lipid accumulation)
PIT=pathological intimal thickening (foam cells, SMC, connective tissue, and extracellular lipid without necrotic core formation)
FA=fibroatheroma (necrotic core formation somewhere)
Calcium: presence of calcium assessed in HE stained sections
Microvessels: Normally, there are some microvessels (vasa vasorum) in adventitia, scored as (+). Abnormal microvessels scored + to +++

122 Vavuranakis et al.
Vasa vasorum imaging by contrast enhanced IVUS

Anatol J Cardiol 2018; 20: 117-24
DOI:10.14744/AnatolJCardiol.2018.35761

software (ACES™) for analysis of CE-IVUS data. In particular, it was shown that the levels of d_MEIR (an operator-independent index of plaque and/or adventitial neovascularization density) were significantly higher in segments with denser VV and/or neovessels, as assessed by histological examination.

CEUS is an emerging technique that has also been utilized for indirect microvessel density assessment of atherosclerotic plaques, primarily in the context of research purposes (3). Indeed, a recent meta-analysis by Huang et al. (12) supports a strong correlation between CEUS findings (plaque enhancement) and microvascular density assessed by histological examination. However, because of ethical and methodological issues, only few, small-sized studies incorporate both ultrasonographic and histological data assessment. Moreover, a series of other limitations have been a point of dispute (30). The automated quantification of VV by computational methods is very limited and the validity of the few existing tools is unexplored. Because of technical, anatomical, and technological limitations, all available imaging modalities for VV visualization and quantification remain under investigation. Therefore, the present study provides valuable additive data on this vague field, in view of both the raw findings per se (correlation of CEUS with histological analysis) and of the novel proposed automated software.

First, there is a profound lack of standardization regarding CEUS methodology. A major point of discrepancy is the protocol utilized for "interpretation" of CEUS raw data. The suggested protocols of image analysis vary from objective, operator dependent, identification of plaque enhancement during CEUS, to automated, operator-independent, software mediated (31). Accordingly, qualitative or semiquantitative descriptions of intraplaque neovascularization have been suggested. However, intraoperator variability remains the most critical issue in the nonautomated protocols.

With regard to studies that incorporated histological evaluation, the exact matching of the excised specimens with the ones that have been utilized for image analysis has also been a point of argument. This undoubtedly diminishes the capability for a high positive predictive value of the technique (32), while it might also partially explain the observed inconsistencies between studies. Indeed, this uncertainty is to be attributed to the two-dimensional approach of current CEUS systems. Future integration of three-dimensional vessel reconstruction may resolve this inherent deficiency (3). Nevertheless, in view of the aforementioned issue, in the present experimental study, surgical clip implantation under ultrasonography guidance guaranteed the exact matching of the specimen histologically analyzed with the one that was visualized under CEUS. Therefore, we may support that our observations provide a sound pathophysiological proof of concept for intraplaque neovascularization identification by CEUS. However, the small sample size of the study should be acknowledged as a limitation, although the collected data were adequate to provide an initial proof of concept for the method under investigation.

On the other hand, not all plaque types "behave" the same way when examined by CEUS. In a recent study by our group

(33), 14 patients scheduled for carotid endarterectomy were evaluated under CEUS and plaques were histologically/immunohistochemically evaluated after excision. Interestingly, brightness enhancement correlated with plaque neovascularization for stable plaques but not for unstable ones. This may imply that additional mechanisms, like plaque fissures that allow direct microbubble entrance to the plaque, also contribute to the final image enhancement.

Another parameter that might influence the accuracy of VV imaging and especially the quantification of VV/neovascularization is the reproducibility of (a) the CE-IVUS technique per se and (b) the computation of d_MEIR metric. Unfortunately, in the present study, we did not perform repeated infusions of the contrast agent and repeated computational analysis of preinfusion and postinfusion IVUS image sequences. Therefore, it was not possible to assess the interobserver and intraobserver reproducibility of the examined method.

In our experimental study, all animals were fed with the atherogenic diet but only four animals received a balloon-induced injury of the aortic endothelium; the remaining six animals did not receive any intervention. Our purpose was to trigger atherosclerotic processes by using different stimuli mechanisms, aiming to develop a variety of atherosclerotic lesions with different characteristics. However, the small sample size did not allow the comparison of atherosclerotic plaque features between these two subgroups.

To conclude, CEUS findings may today appear as another point in the shortlisting of vulnerable plaque features. Indeed, vulnerable plaque hunting has changed the last few years, leading to a redefinition of this entity from "A plaque with specific morphological features—usually referring exclusively to thin cap fibroatheromas" to "A plaque that is prone to rupture when all intrinsic and extrinsic effects are taken into account (regardless of structure)" (3).

The potential clinical relevance of our findings first relates to the histological verification of the ability of this new method to detect and quantify VV and neovascularization *in vivo* at atherosclerotic vessels. Through CE-IVUS and proper imaging analysis algorithms, it is possible to further determine another critical parameter for plaque vulnerability and progression (i.e., neovascularization). Therefore, the proposed technique could provide an additional biomarker/tool to assess plaque vulnerability. However, further clinical studies in humans should explore the prognostic role of this new metric as well as its ability to drive decision making concerning the treatment of atherosclerotic vessels.

Conclusion

It is possible to detect vasa vasorum or neovascularization *in vivo* using computational analysis of CE-IVUS images, which is in agreement with histological data. A semiquantitative grading of VV/neovascularization seems to more appropriate approach.

Anatol J Cardiol 2018; 20: 117-24
DOI:10.14744/AnatolJCardiol.2018.35761

Vavuranakis et al.
Vasa vasorum imaging by contrast enhanced IVUS   *123*

These findings may have critical implications on vulnerable plaque assessment and risk stratification. Regardless, the predictive and prognostic value of the quantitative assessment of VV proliferation or plaque neovascularization concerning patients' outcome and coronary adverse events needs confirmation in future clinical studies.

Ethical issues: The experimental protocol was approved by the local ethics committee (Athens Prefecture Veterinarian Service); competent veterinary services ensured harmonization to the European Union Directive 2010/63/EU. Animals were handled according to the guidelines of the Guide for the Care and Use of Laboratory Animals of the US National Research Council Tissue Preparation.

Conflict of interest: None declared.

Peer-review: Externally peer-reviewed.

Authorship contributions: Concept – M.V., T.G.P., I.K.; Design – M.V., M.K., S.V., C.S.; Supervision – C.S., D.T.; Fundings – M.K., G.A., E.P; Materials – M.K., G.A., E.P; Data collection &/or processing – M.V., E.A.S., S.V., G.A., E.P.; Analysis &/or interpretation – M.V., E.A.S., G.A.; Literature search – D.V., E.A.S., I.K.; Writing – M.V., T.G.P., E.A.S.; Critical review – M.V., I.K., C.S., D.T.

References

1. Virmani R, Ladich ER, Burke AP, Kolodgie FD. Histopathology of carotid atherosclerotic disease. Neurosurgery 2006; 59(5 Suppl 3): S219-27. [CrossRef]

2. Finn AV, Nakano M, Narula J, Kolodgie FD, Virmani R. Concept of vulnerable/unstable plaque. Arterioscler Thromb Vasc Biol 2010;30: 1282-92. [CrossRef]

3. Stefanadis C, Antoniou CK, Tsiachris D, Pietri P. Coronary Atherosclerotic Vulnerable Plaque: Current Perspectives. J Am Heart Assoc 2017; 6: pii: e005543. [CrossRef]

4. Moreno PR, Purushothaman KR, Fuster V, Echeverri D, Truszczynska H, Sharma SK, et al. Plaque neovascularization is increased in ruptured atherosclerotic lesions of human aorta: implications for plaque vulnerability. Circulation 2004; 110: 2032-8. [CrossRef]

5. Carlier S, Kakadiaris IA, Dib N, Vavuranakis M, O'Malley SM, Gul K, et al. Vasa vasorum imaging: A new window to the clinical detection of vulnerable atherosclerotic plaques. Curr Atheroscler Rep 2005; 7: 164-9. [CrossRef]

6. Fleiner M, Kummer M, Mirlacher M, Sauter G, Cathomas G, Krapf R, et al. Arterial neovascularization and inflammation in vulnerable patients: early and late signs of symptomatic atherosclerosis. Circulation 2004; 110: 2843-50. [CrossRef]

7. Giannoni MF, Vicenzini E, Citone M, Ricciardi MC, Irace L, Laurito A, et al. Contrast carotid ultrasound for the detection of unstable plaques with neoangiogenesis: a pilot study. Eur J Vasc Endovasc Surg 2009; 37: 722-7. [CrossRef]

8. Staub D, Patel MB, Tibrewala A, Ludden D, Johnson M, Espinosa P, et al. Vasa vasorum and plaque neovascularization on contrast-enhanced carotid ultrasound imaging correlates with cardiovascular disease and past cardiovascular events. Stroke 2010; 41: 41-7.

9. Jorgensen SM, Korinek MJ, Vercnocke AJ, Anderson JL, Halaweish A, Leng S, et al. Arterial Wall Perfusion Measured with Photon Counting Spectral X-ray CT. Proc SPIE Int Soc Opt Eng 2016; 9967.

10. Kerwin WS, Oikawa M, Yuan C, Jarvik GP, Hatsukami TS. MR imaging of adventitial vasa vasorum in carotid atherosclerosis. Magn Reson Med 2008; 59: 507-14. [CrossRef]

11. Osborn EA, Jaffer FA. Imaging inflammation and neovascularization in atherosclerosis: clinical and translational molecular and structural imaging targets. Curr Opin Cardiol 2015; 30: 671-80.

12. Huang R, Abdelmoneim SS, Ball CA, Nhola LF, Farrell AM, Feinstein S, et al. Detection of Carotid Atherosclerotic Plaque Neovascularization Using Contrast Enhanced Ultrasound: A Systematic Review and Meta-Analysis of Diagnostic Accuracy Studies. J Am Soc Echocardiogr 2016; 29: 491-502. [CrossRef]

13. Johri AM, Herr JE, Li TY, Yau O, Nambi V. Novel Ultrasound Methods to Investigate Carotid Artery Plaque Vulnerability. J Am Soc Echocardiogr 2017; 30: 139-48. [CrossRef]

14. Vavuranakis M, Kakadiaris IA, O'Malley SM, Papaioannou TG, Sanidas EA, Naghavi M, et al. A new method for assessment of plaque vulnerability based on vasa vasorum imaging, by using contrast-enhanced intravascular ultrasound and differential image analysis. Int J Cardiol 2008; 130: 23-9. [CrossRef]

15. Goertz DE, Frijlink ME, Tempel D, Bhagwandas V, Gisolf A, Krams R, et al. Subharmonic contrast intravascular ultrasound for vasa vasorum imaging. Ultrasound Med Biol 2007; 33: 1859-72. [CrossRef]

16. Goertz DE, Frijlink ME, Krams R, de Jong N, van der Steen AF. Vasa vasorum and molecular imaging of atherosclerotic plaques using nonlinear contrast intravascular ultrasound. Neth Heart J 2007; 15: 77-80. [CrossRef]

17. O'Malley SM, Vavuranakis M, Naghavi M, Kakadiaris IA. Intravascular ultrasound-based imaging of vasa vasorum for the detection of vulnerable atherosclerotic plaque. Med Image Comput Comput Assist Interv 2005; 8: 343-51. [CrossRef]

18. Ruiz EM, Papaioannou TG, Vavuranakis M, Stefanadis C, Naghavi M, Kakadiaris IA. Analysis of contrast-enhanced intravascular ultrasound images for the assessment of coronary plaque neoangiogenesis: another step closer to the identification of the vulnerable plaque. Curr Pharm Des 2012; 18: 2207-13. [CrossRef]

19. Vavuranakis M, Kakadiaris IA, Papaioannou TG, O'Malley SM, Carlier S, Naghavi M, et al. Contrast-enhanced intravascular ultrasound: combining morphology with activity-based assessment of plaque vulnerability. Expert Rev Cardiovasc Ther 2007; 5: 917-25. [CrossRef]

20. Vavuranakis M, Papaioannou TG, Kakadiaris IA, O'Malley SM, Naghavi M, Filis K, et al. Detection of perivascular blood flow in vivo by contrast-enhanced intracoronary ultrasonography and image analysis: An animal study. Clin Exp Pharmacol Physiol 2007; 34: 1319-23. [CrossRef]

21. O'Malley SM, Vavuranakis M, Naghavi M, Kakadiaris IA. Intravascular ultrasound-based imaging of vasa vasorum for the detection of vulnerable atherosclerotic plaque. Med Image Comput Comput Assist Interv 2005; 8:343-51. [CrossRef]

22. O'Malley SM, Granada JF, Carlier S, Naghavi M, Kakadiaris IA. Image-based gating of intravascular ultrasound pullback sequences. IEEE Trans Inf Technol Biomed 2008; 12: 299-306. [CrossRef]

23. Gonzalo N, Serruys PW, Garcia-Garcia HM, van Soest G, Okamura T, Ligthart J, et al. Quantitative ex vivo and in vivo comparison of lumen dimensions measured by optical coherence tomography and intravascular ultrasound in human coronary arteries. Rev Esp Cardiol 2009; 62: 615-24. [CrossRef]

124 Vavuranakis et al.
Vasa vasorum imaging by contrast enhanced IVUS

Anatol J Cardiol 2018; 20: 117-24
DOI:10.14744/AnatolJCardiol.2018.35761

24. Exarchos KP, Carpegianni C, Rigas G, Exarchos TP, Vozzi F, Sakellarios A, et al. A multiscale approach for modeling atherosclerosis progression. IEEE J Biomed Health Inform 2015; 19: 709-19. [CrossRef]

25. Lu Y, Wei J, Shao Q, Tang Y, Huang Y, Zhang H, et al. Assessment of atherosclerotic plaques in the rabbit abdominal aorta with interleukin-8 monoclonal antibody-targeted ultrasound microbubbles. Mol Biol Rep 2013; 40: 3083-92. [CrossRef]

26. Zhang G, Li M, Li L, Xu Y, Li P, Yang C, et al. The immunologic injury composite with balloon injury leads to dyslipidemia: a robust rabbit model of human atherosclerosis and vulnerable plaque. J Biomed Biotechnol 2012; 2012: 249129. [CrossRef]

27. Tanaka H, Sukhova GK, Swanson SJ, Clinton SK, Ganz P, Cybulsky MI, et al. Sustained activation of vascular cells and leukocytes in the rabbit aorta after balloon injury. Circulation 1993; 88: 1788-803.

28. Martina JD, Simmons C, Jukic DM. High-definition hematoxylin and eosin staining in a transition to digital pathology. J Pathol Inform 2011; 2: 45. [CrossRef]

29. Virmani R, Narula J, Leon MB, Willerson JT. The Vulnerable Atherosclerotic Plaque: Strategies for Diagnosis and Management. Wiley, Blackwell Publishing; 2007.

30. Vrachatis DA, Papaioannou TG, Vavuranakis M, Tousoulis D. In Vivo Assessment of Atherosclerotic Plaque Neovascularization by Contrast-Enhanced Ultrasound: An Unsolved Mystery? J Am Soc Echocardiogr 2017; 30: 724. [CrossRef]

31. Staub D, Schinkel AF, Coll B, Coli S, van der Steen AF, Reed JD, Krueger C, et al. Contrast-enhanced ultrasound imaging of the vasa vasorum: from early atherosclerosis to the identification of unstable plaques. JACC Cardiovasc Imaging 2010; 3: 761-71. [CrossRef]

32. Shah F, Balan P, Weinberg M, Reddy V, Neems R, Feinstein M, et al. Contrast-enhanced ultrasound imaging of atherosclerotic carotid plaque neovascularization: a new surrogate marker of atherosclerosis? Vasc Med 2007; 12: 291-7. [CrossRef]

33. Vavuranakis M, Sigala F, Vrachatis DA, Papaioannou TG, Filis K, Kavantzas N, et al. Quantitative analysis of carotid plaque vasa vasorum by CEUS and correlation with histology after endarterectomy. Vasa 2013; 42: 184-95. [CrossRef]